JGR Oceans

RESEARCH ARTICLE
10.1029/2021JC017429

Key Points:

- Observations and simulations suggest substantial intraseasonal variability in the deep flow over slopes of the northern South China Sea
- Deep-flow variability is dynamically linked to the Kuroshio intrusion and related eddies via topographic Rossby waves
- This study highlights an energy pathway from the open ocean into the abyssal marginal sea that could be critical to the global energy budget

Correspondence to:
Z. Liu,
liuzq@sustech.edu.cn

Citation:
Quan, Q., Liu, Z., Sun, S., Cai, Z., Yang, Y., Jin, G., et al. (2021). Influence of the Kuroshio intrusion on deep flow intraseasonal variability in the northern South China Sea. *Journal of Geophysical Research: Oceans*, *126*, e2021JC017429. https://doi.org/10.1029/2021JC017429

Received 31 MAR 2021
Accepted 20 JUN 2021

Influence of the Kuroshio Intrusion on Deep Flow Intraseasonal Variability in the Northern South China Sea

Qi Quan[1], Zhiqiang Liu[1], Shantong Sun[2], Zhongya Cai[3,4], Yang Yang[5], Guangzhen Jin[6], Zhibing Li[1], and X. San Liang[5]

[1]Department of Ocean Science and Engineering, Southern University of Science and Technology, Shenzhen, China, [2]Environmental Science and Engineering, California Institute of Technology, Pasadena, CA, USA, [3]State Key Laboratory of Internet of Things for Smart City and Department of Civil and Environmental Engineering, University of Macau, Macau, China, [4]Center for Ocean Research in Hongkong and Macau, Macau, China, [5]School of Marine Sciences, Nanjing University of Information Science and Technology, Nanjing, China, [6]College of Marine Ecology and Environment, Shanghai Ocean University, Shanghai, China

Abstract Interactions between the open ocean and marginal seas have been suggested to be critical to the redistribution and dissipation of global energy. Here, we propose a mechanism for the upper open ocean influencing the deep flow in marginal seas that hinges on the formation and propagation of topographic Rossby waves (TRWs). Observations and high-resolution simulations suggest substantial intraseasonal variability with periods of 5–60 days associated with the deep flow over continental slopes of the northern South China Sea (NSCS). These fluctuations generally account for over 40% of the total deep kinetic energy variability and the number can reach 70% over the slopes to the west of the Luzon Strait, southwest of the Dongsha Islands, and northeast of the Xisha Islands. By examining the spatiotemporal features of the fluctuations, we demonstrate that the intraseasonal variability of the deep flow in the NSCS is closely associated with TRWs. Using a recently developed multiscale energetics analysis in combination with a ray tracing model, we show that the energy sources of TRWs can be traced back to the east of the Dongsha Islands, where the Kuroshio intrusion and related eddies energize the TRWs primarily through pressure work. These waves propagate westward across the NSCS and drive the intraseasonal variability of the deep flow over continental slopes. Our findings highlight an energy pathway from the open ocean western boundary current to the abyssal marginal sea that could modulate regional circulation as well as exchanges between major ocean basins.

Plain Language Summary The Kuroshio intrusion can substantially modulate the circulation of the South China Sea (SCS), affecting the Indo-Pacific exchange, climate, and ecosystem. Traditionally, its dynamic impact is thought to be confined to the upper layer. However, in this study, we propose a mechanism that links the Kuroshio to deep processes in the northern SCS (NSCS). We suggest that the deep flow intraseasonal variability over the continental slopes of the NSCS could be dynamically tied to the Kuroshio intrusion and related eddies via topographic Rossby waves. The results highlight an energy pathway from the upper open ocean to the abyssal marginal sea, which could be critical to the redistribution and dissipation of global energy.

1. Introduction

The dynamic coupling between the open ocean and marginal seas has been suggested to be critical to the redistribution and dissipation of global energy (Ferrari & Wunsch, 2009). Here, we focus on the interactions between the South China Sea (SCS) and Kuroshio intrusion, which carries energy from the Pacific Ocean into the SCS (Nan et al., 2015). Recently, Quan et al. (2021) revealed the presence of energetic topographic Rossby waves (TRWs) in the abyssal SCS (>2,000 m), which contribute greatly to the intraseasonal variability of the deep flow over continental slopes. In this study, we show that the Kuroshio intrusion and related eddies serve as an important energy source for the TRWs in the northern South China Sea (NSCS), which are energized via pressure work and propagate along continental slopes to drive the deep-flow variability (Figure 1).

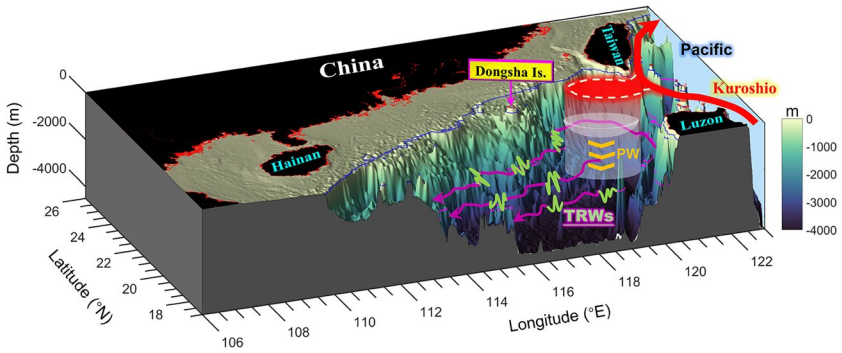

Figure 1. Schematic of the dynamic linkage between the Kuroshio intrusion and deep flow intraseasonal variability in the northern South China Sea. The region where the Kuroshio intrusion occurs is highlighted by the red area. The Kuroshio intrusion and related eddies energize the topographic Rossby waves (magenta rays) via pressure work (PW; yellow arrows). These waves propagate along the continental slopes and drive the intraseasonal variability in the deep flow (represented by the pulse-like green lines).

The Kuroshio originates from the North Equatorial Current and intrudes into the SCS via the Luzon Strait (Figure 2a). As a primary component of the SCS throughflow, the Kuroshio intrusion comprises of a major pathway for water exchange between the Pacific Ocean and SCS, substantially constraining the dynamic and thermodynamic states of the SCS (Gan et al., 2016; Qu et al., 2006, 2009; Xue et al., 2004; Yu et al., 2007). The Kuroshio intrusion has also been suggested to modulate the Indonesian throughflow, which is the only low-latitude oceanic pathway for freshwater and heat exchange between major ocean basins (Gordon et al., 2012; Wei et al., 2016).

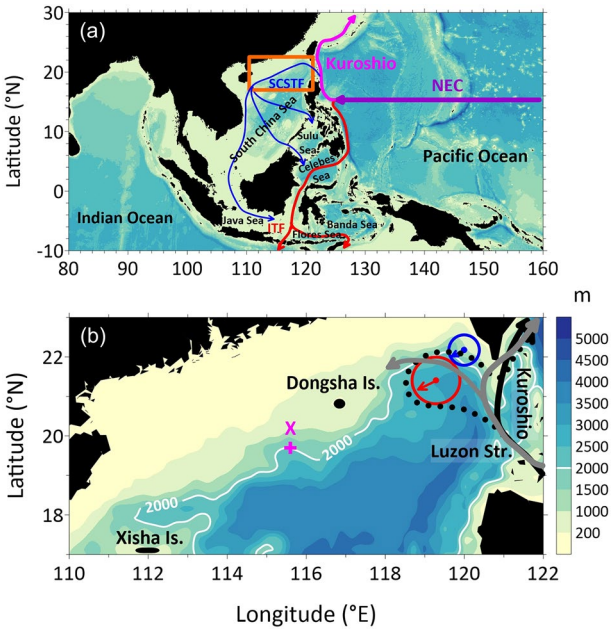

Figure 2. (a) Schematic of the North Equatorial Current (purple), Kuroshio (magenta), South China Sea throughflow (blue), and Indonesian throughflow (red). The northern South China Sea (NSCS) is highlighted by the orange rectangle. (b) Topography (m) of the NSCS. The solid, dashed, and gray streamlines denote the leaping, looping, and leaking paths of the Kuroshio intrusion, respectively. The red circle denotes the anticyclonic loop current eddy shedding from the Kuroshio mainstream, which is usually accompanied with a cyclonic eddy (blue circle) moving southwestward. The magenta cross indicates the mooring site X.

Because the dynamic impacts of the Kuroshio intrusion are most prominent to the north of 17°N, the NSCS (orange rectangle in Figure 2a), defined as the region between 17°–23°N and 110°–121°E, is typically recognized as a region that is dynamically distinct from the other parts of the SCS (Quan et al., 2016; Shu et al., 2018; Wang, Zeng, Shu, et al., 2020; Xu & Oey, 2015). The Kuroshio intrusion into the NSCS is mainly confined to the upper 500 m (J. Tian et al., 2006; Q. Yang et al., 2010; Zhang et al., 2015) and usually occurs in three characteristic forms (Figure 2b; Nan et al., 2011a). The instability associated with the Kuroshio near the Luzon Strait can result in frequent mesoscale eddy shedding (Zhang et al., 2013, 2017), which has been suggested to contribute greatly to the eddy activity and intraseasonal variability of the upper-layer flow in the NSCS (Chen et al., 2011; Wang, Zeng, Chen, et al., 2020; Wang, Zhou, et al., 2020; Xiu et al., 2010). In this study, we demonstrate that the Kuroshio intrusion and related eddies in the upper layer also contribute to the intraseasonal variability of the deep flow in the NSCS.

In marginal seas with an open ocean western boundary current (WBC) intrusion, the deep-flow variability has often been linked to the formation of deep ocean eddies through baroclinic instability of the WBC intrusion, or been explained through potential vorticity (PV) adjustments to changing depth of the bottom and the interface between layers (e.g., Donohue et al., 2016; Hamilton, 2009; Hamilton et al., 2019; Oey, 2008). Here, we argue from an energetic perspective using a multiscale energy analysis and show that the WBC intrusion and related eddies can directly drive the deep flow intraseasonal variability through pressure work, which is closely associated with the work done by interfacial form stress (Johnson & Bryden, 1989).

The structure of this paper is as follows. In Section 2, we describe the data and methods employed. In Section 3.1, we examine deep-flow variability using a single mooring and high-resolution simulations. Then, we investigate the key energetics in Section 3.2. To illustrate the underlying dynamics, we discuss a representative event as an example in Section 3.3. Finally, a summary is provided in Section 4.

2. Data and Methods

2.1. Data

In this study, we use a deep mooring to reveal the bottom flow variability in the NSCS. The mooring site X was on the continental slope to the southwest of Dongsha Islands (magenta cross in Figure 2b), where the water depth is ~2,000 m. An upward looking 600 kHz acoustic Doppler current profiler was employed with four observational depths (1,981.62, 1,986.62, 1,991.62, and 1,996.62 m). The sampling time interval was 0.5 h. Velocity profiles were continuously recorded for approximately 8 months from August 12, 2011 to April 12, 2012, and the percentage of valid data was higher than 95%. Because of the viscous effects in the bottom boundary layer, velocities at the four levels are basically in phase but decrease in magnitude downward (not shown). This would obscure the inviscid TRWs dynamics (Rhines, 1970), in which the wave-induced velocity is bottom-intensified. Hence, we just analyze the data at the top level (1,981.62 m; ~20 m above the bottom) to investigate the period and directivity of the deep-flow variability.

To identify and track the mesoscale eddies in the NSCS, the daily merged sea level anomaly (SLA) obtained with the satellite altimeters from the Copernicus Marine Environment Monitoring Service, with a horizontal resolution of 1/4°, is used in combination with the efficient parallel identification and optimized tracking algorithms (F. Tian et al., 2020).

Because of the limited spatial and temporal coverage of the observations, we also use the 6 years output from the Hybrid Coordinate Ocean Model (HYCOM) + Navy Coupled Ocean Data Assimilation global 1/12° Analysis (GLBv0.08; Cummings & Smedstad, 2013), from 2013 to 2018, to examine the processes that lead to the observed deep-flow variability. This data set covers a sufficiently long period to resolve the intraseasonal motions and has been validated to reproduce multiscale processes in the SCS (e.g., Shu et al., 2014; Sun et al., 2020; Wang, Zeng, Chen, et al., 2020). The 3-h data set has a horizontal resolution of about 8.4–9.2 km at 5°–25°N and 41 vertical levels from 0 to 5,500 m (1,000, 1,250, 1,500, 2,000, 2,500, 3,000, 4,000, 5,000, and 5,500 m for the deep layer).

The HYCOM reanalysis data have been widely employed in the multiscale energy analysis of the world oceans, such as the available potential energy (APE) field in the global ocean, energetics of eddy-mean flow interactions in the Brazil Current, seasonal cycle of the eddy kinetic energy (KE) in the Kuroshio Extension, and energy transfer underlying the eddy shedding from the Kuroshio in the northeastern SCS (Luecke et al., 2017; Magalhães et al., 2017; Yang & Liang, 2018; Zhang et al., 2017). Note that the HYCOM reanalysis is close to a free-running case in the SCS because the available observations in this region are too limited for data assimilation (Cummings & Smedstad, 2013). Hence, the model is largely consistent by kinematics and dynamics in the SCS, which is feasible for the energetics analysis in our study.

2.2. Multiscale Energy Analysis in a Three-Window Framework

To determine the energy source of the deep flow variability, we adopt the method of multiscale energy and vorticity analysis (MS-EVA; Liang, 2016) to investigate the energetics of the abyssal NSCS. This method has been successfully employed in previous studies to evaluate multiscale oceanic and atmospheric energy budgets (Liang & Robinson, 2009; Ma & Liang, 2017; Yang & Liang, 2016, 2018; Y. Yang et al., 2020). The MS-EVA is based on the multiscale window transform (MWT; Liang & Anderson, 2007), to decompose a function space into a sum of several orthogonal subspaces called scale windows, each with an exclusive timescale range. In a three-window framework (denoted by $\varpi = 0, 1, 2$), a given time series $R(t)$ can be reconstructed as:

$$R^{\sim\varpi}(t) = \sum_{n=0}^{2^{j_2}-1} \hat{R}_n^{\sim\varpi} \phi_n^{j_2}(t), \quad \varpi = 0, 1, 2, \tag{1}$$

where $\hat{R}_n^{\sim\varpi} = \int_0^1 R^{\sim\varpi}(t)\phi_n^{j_2}(t)dt$ is the MWT coefficient and $\left\{\phi_n^j(t)\right\}_n$ is an orthonormal scaling function basis constructed by Liang and Anderson (2007), with j ($j_0 < j_1 < j_2$) being the scale level and n ($n = 0, 1,..., 2^{j_2} - 1$) being the sampling time step. Using this method, the original HYCOM reanalysis data are split into three scale windows: the nonstationary background flow window (>128 days; $\varpi = 0$), the intraseasonal fluctuation window (8–128 days; $\varpi = 1$), and the high-frequency oscillation window (<8 days; $\varpi = 2$). We use 8–128 days instead of 5–90 days, which is the normal definition of the intraseasonal timescale in the SCS (Wang, Zhou, et al., 2020), because the window bounds can only be an exponential function of base two in the MS-EVA method.

Employing the MS-EVA to investigate the dynamics of a hydrostatic Boussinesq fluid flow, we obtain the mechanical energy equation on window ϖ:

$$\frac{\partial\left(K^{\varpi} + A^{\varpi}\right)}{\partial t} = \Delta Q_K^{\varpi} + \Delta Q_A^{\varpi} + \Delta Q_P^{\varpi} + \Gamma_K^{\varpi} + \Gamma_A^{\varpi} + F_K^{\varpi} + F_A^{\varpi}, \tag{2}$$

where K^{ϖ} and A^{ϖ} represent KE and APE, respectively, ΔQ_K^{ϖ} (ΔQ_A^{ϖ}) is the KE (APE) transport by advection, ΔQ_P^{ϖ} is the pressure work related to the distorted isopycnals, Γ_K^{ϖ} (Γ_A^{ϖ}) is the KE (APE) transfer, the residual terms F_K^{ϖ} and F_A^{ϖ} (not explicitly expressed) include contributions from external forcing, friction, and other unresolved subgrid processes. Note that the cross-scale transfers Γ^{ϖ}, which correspond precisely to the classical instability theory (Liang & Robinson, 2007), need to be further decomposed to obtain the interactions between windows within the three-window framework, by a technique called "interaction analysis" (Liang & Robinson, 2005). For example, the transfer of KE (APE) from the background flow window ($\varpi = 0$) to the intraseasonal fluctuation window ($\varpi = 1$) is denoted as $\Gamma_K^{0\to1}$ ($\Gamma_A^{0\to1}$). A positive $\Gamma_K^{0\to1}$ ($\Gamma_A^{0\to1}$) means a forward energy cascade, which is indicative of barotropic (baroclinic) instability. Similarly, interactions between windows $\varpi = 1$ and $\varpi = 2$ ($\varpi = 0$ and $\varpi = 2$) are quantified by $\Gamma^{1\to2}$ ($\Gamma^{0\to2}$). The cross-scale transfers Γ^{ϖ} satisfy the following property:

$$\sum_{\varpi}\sum_{n} \Gamma_n^{\varpi} = 0, \tag{3}$$

where Σ_{ϖ} and Σ_n sum over all the scale windows and sampling time steps n, respectively. This critical property guarantees that transfer should be a mere redistribution of energy among scale windows, without generating or losing energy as a whole. For this reason, it is called a *canonical transfer*, in contrast to those defined in previous literature. The expressions for each term in Equation 2 are listed in Table 1 and the detailed derivation can be referred to Liang (2016). In the following, we will focus on the energetics on the window $\varpi = 1$.

2.3. Ray Tracing Model

To investigate the propagation and the possible energy source of the TRWs in the deep NSCS, we use a ray-tracing technique. The model is modified from that in Meinen et al. (1993) by considering the background flow. In accordance with Oey and Lee (2002), the equations governing the raypath and wavenumber are:

$$\frac{d\mathbf{x}}{dt} = \frac{\partial\omega}{\partial\mathbf{K}} = \mathbf{C}_g + \mathbf{v}_h, \tag{4}$$

$$\frac{d\mathbf{K}}{dt} = -\sum_{i=1}^{n} \frac{\partial\omega}{\partial E_i}\nabla E_i - k\nabla u - l\nabla v, \tag{5}$$

Table 1
Expression and Physical Meaning of Each Term in Equation 2

Term	Expression	Physical meaning
K^{ϖ}	$\frac{1}{2}\hat{\mathbf{v}}_h^{\sim\varpi}\cdot\hat{\mathbf{v}}_h^{\sim\varpi}$	KE on window ϖ; $\mathbf{v}$ is the velocity vector
ΔQ_K^{ϖ}	$-\nabla\cdot\left[\frac{1}{2}(\widehat{\mathbf{v}\mathbf{v}_h})^{\sim\varpi}\cdot\hat{\mathbf{v}}_h^{\sim\varpi}\right]$	KE transport on window ϖ
Γ_K^{ϖ}	$\frac{1}{2}\left[(\widehat{\mathbf{v}\mathbf{v}_h})^{\sim\varpi}:\nabla\hat{\mathbf{v}}_h^{\sim\varpi}-\nabla\cdot(\widehat{\mathbf{v}\mathbf{v}_h})^{\sim\varpi}\cdot\hat{\mathbf{v}}_h^{\sim\varpi}\right]$	Canonical KE transfer to window ϖ
ΔQ_P^{ϖ}	$-\nabla\cdot\left(\frac{1}{\rho_0}\hat{\mathbf{v}}^{\sim\varpi}\hat{P}^{\sim\varpi}\right)$	Pressure work on window ϖ; P is the dynamic pressure related to ρ; ρ_0 is the reference density of seawater
A^{ϖ}	$\frac{1}{2}c\left(\hat{\rho}^{\sim\varpi}\right)^2, c=\frac{g^2}{\rho_0^2N^2}$	APE on window ϖ; ρ is the density anomaly from a reference state $\rho_r(z)$; g is the gravitational acceleration; N is the buoyancy frequency
ΔQ_A^{ϖ}	$-\nabla\cdot\left[\frac{1}{2}c\hat{\rho}^{\sim\varpi}\left(\widehat{\mathbf{v}\rho}\right)^{\sim\varpi}\right]$	APE transport on window ϖ
Γ_A^{ϖ}	$\frac{c}{2}\left[\left(\widehat{\mathbf{v}\rho}\right)^{\sim\varpi}\cdot\nabla\hat{\rho}^{\sim\varpi}-\hat{\rho}^{\sim\varpi}\nabla\cdot\left(\widehat{\mathbf{v}\rho}\right)^{\sim\varpi}\right]$	Canonical APE transfer to window ϖ

Note. The colon operator is defined such that, for two dyadic products **AB** and **CD**, $(\mathbf{AB}):(\mathbf{CD})=(\mathbf{A}\cdot\mathbf{C})(\mathbf{B}\cdot\mathbf{D})$.
Abbreviations: APE, available potential energy; KE, kinetic energy.

where $(d/dt)=(\partial/\partial t)+(\mathbf{C}_g+\mathbf{v}_h)\cdot\nabla$ is the derivative following the wave group, ω is the frequency, $\mathbf{x}$ is the location of the wave group (i.e., the energy ray), $\mathbf{C}_g$ is the group velocity, $\mathbf{v}_h=(u,v)$ is the horizontal background flow, $\mathbf{K}=(k,l)$ is the horizontal wavenumber vector, and E_i denotes any of the environmental parameters, such as the buoyancy frequency N, water depth h, and topographic gradient ∇h, that result in wave refraction. Given the initial position, frequency, wavenumber vector, environmental parameters, and background flow, Equations 4 and 5 can be integrated forward or backward in time. Note that the model is under the Wentzel-Kramer-Brillouin limit, where the environmentally induced changes in the wave amplitude and phase are assumed to vary at scales larger than the local wavelength. Hence, we use the smoothed topography and stratification from HYCOM GLBv0.08 for calculation (Hamilton, 2009; Pickart, 1995). We smooth the topography by using a Shapiro filter to eliminate the small-scale undulations. In the deep NSCS, the buoyancy frequency N is a weak function of depth. Thus, the 6-year mean N averaged over the water column 200 m above the bottom is used here.

3. Results

3.1. Intraseasonal Variability of Deep Flow and TRWs in the NSCS

Consistent with the observations to the southeast of the Dongsha Islands (Wang et al., 2019), significant intraseasonal variability of the bottom flow is also observed at site X. Despite strong tidal contributions, the intraseasonal oscillations, filtered by a 5–90 days band-pass, account for 40.2% of the standard deviation (STD) of total KE (Figure 3a). The spectral analysis reveals significant KE associated with the intraseasonal oscillations of periods between 5 and 20 days, above the 95% confidence level (blue line in Figure 3b). Within this significant period band, the STD ellipse of the bottom velocity is characterized by a small oblateness with the major principal axis (approximately 0.02 m s^{-1}; ~30% of the mean flow) parallel to the local isobath (blue ellipse in Figure 3c), indicating that the oscillation direction is primarily along the local isobath, but exhibits considerable deviation.

The HYCOM reanalysis shows features similar to those observed in the significant intraseasonal variability of deep flow in the NSCS. As shown in Figure 3b (orange line), the spectrum of subinertial motions in the HYCOM largely reproduces the observations despite a weaker intensity. Without tidal effects, the modeled intraseasonal

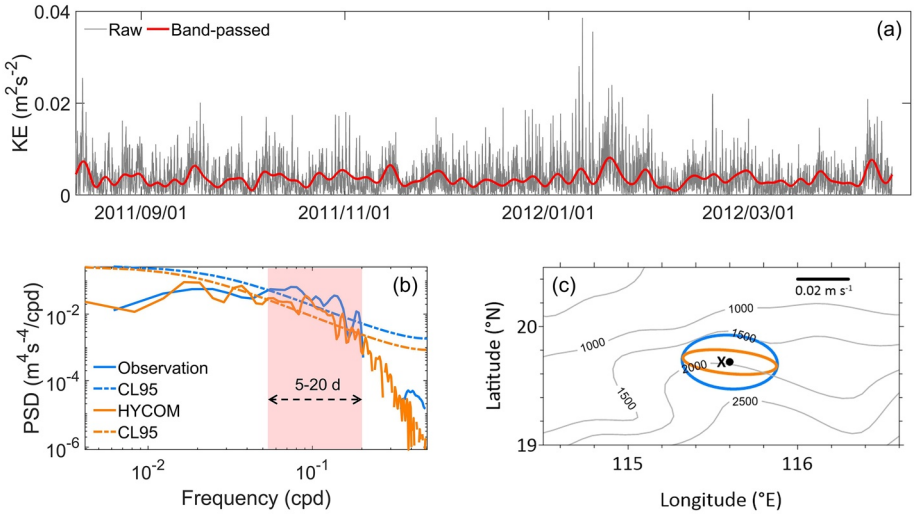

Figure 3. (a) Observed bottom kinetic energy (KE) (m^2 s^{-2}) at site X for raw (gray) and 5–90 days band-passed (red) data. (b) Power spectra of 5–90 days band-passed bottom KE at site X from observations (blue) and Hybrid Coordinate Ocean Model (HYCOM) data (orange). Components significant at the 95% confidence level are shaded. (c) Standard deviation ellipses of 5–20 days band-passed bottom velocity at site X for observations (blue) and HYCOM data (orange). Contours denote the isobaths.

oscillations account for 54.3% of the bottom-KE variability at site X, with the STD ellipse aligned with the observations but more rectilinear (orange ellipse in Figure 3c). Such deep-flow variability is found to occur extensively over the continental slopes in the NSCS, with the periods of 5–60 days at the 95% confidence level (Figure 4a). In these regions, the modeled mean flow near the bottom is weak, at less than 0.05 m s^{-1} (Figure 4b). By contrast, the STD ellipses of the near-bottom velocities (filtered within the local significant period band in Figure 4a) have principal axes comparable to or even larger than the mean flow at six sites along the 3,000 m isobath (where TRWs are identified later). Similar results appear widely over the slopes of the abyssal NSCS (not shown). These

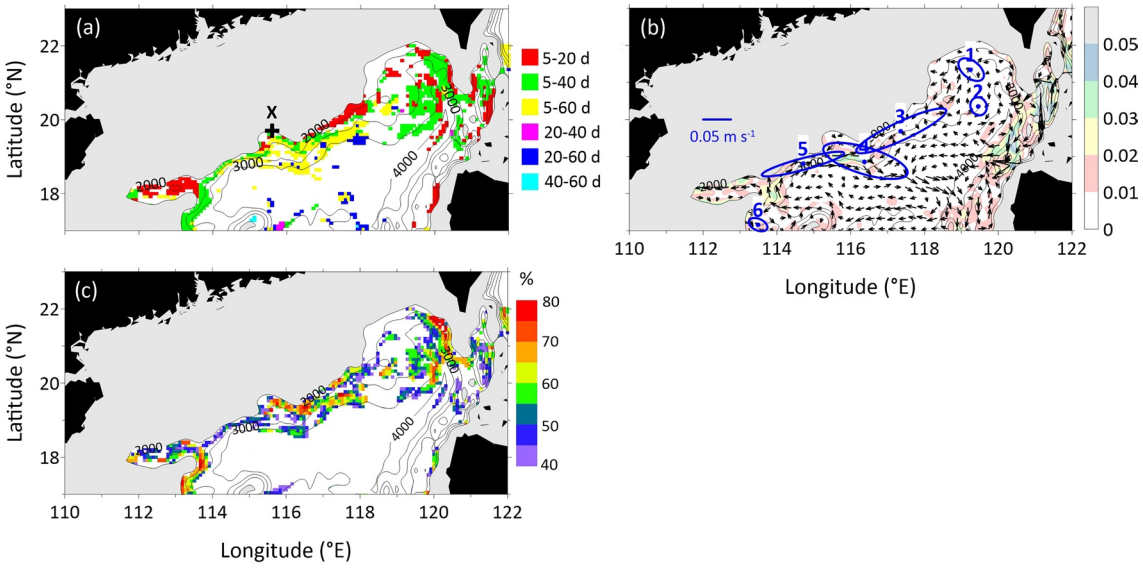

Figure 4. (a) Significant period bands (days) of the depth-integrated kinetic energy (KE) below 2,000 m in the deep northern South China Sea (NSCS) at the 95% confidence level. The white space denotes the locations where the intraseasonal variability of deep-layer KE is not significant. The black cross indicates site X. (b) Climatology of the bottom flow in the NSCS based on HYCOM GLBv0.08. Color shading indicates the speed magnitude (m s^{-1}), and the vectors indicate the flow directions. Standard deviation (STD) ellipses of band-passed bottom velocity (blue) are shown at six sites along the 3,000 m isobath. (c) Ratio between the STD of the intraseasonal deep KE and STD of the total deep KE (integrated from the bottom to 2,000 m using Hybrid Coordinate Ocean Model GLBv0.08) at locations where topographic Rossby waves are identified. Note that areas shallower than 2,000 m are masked.

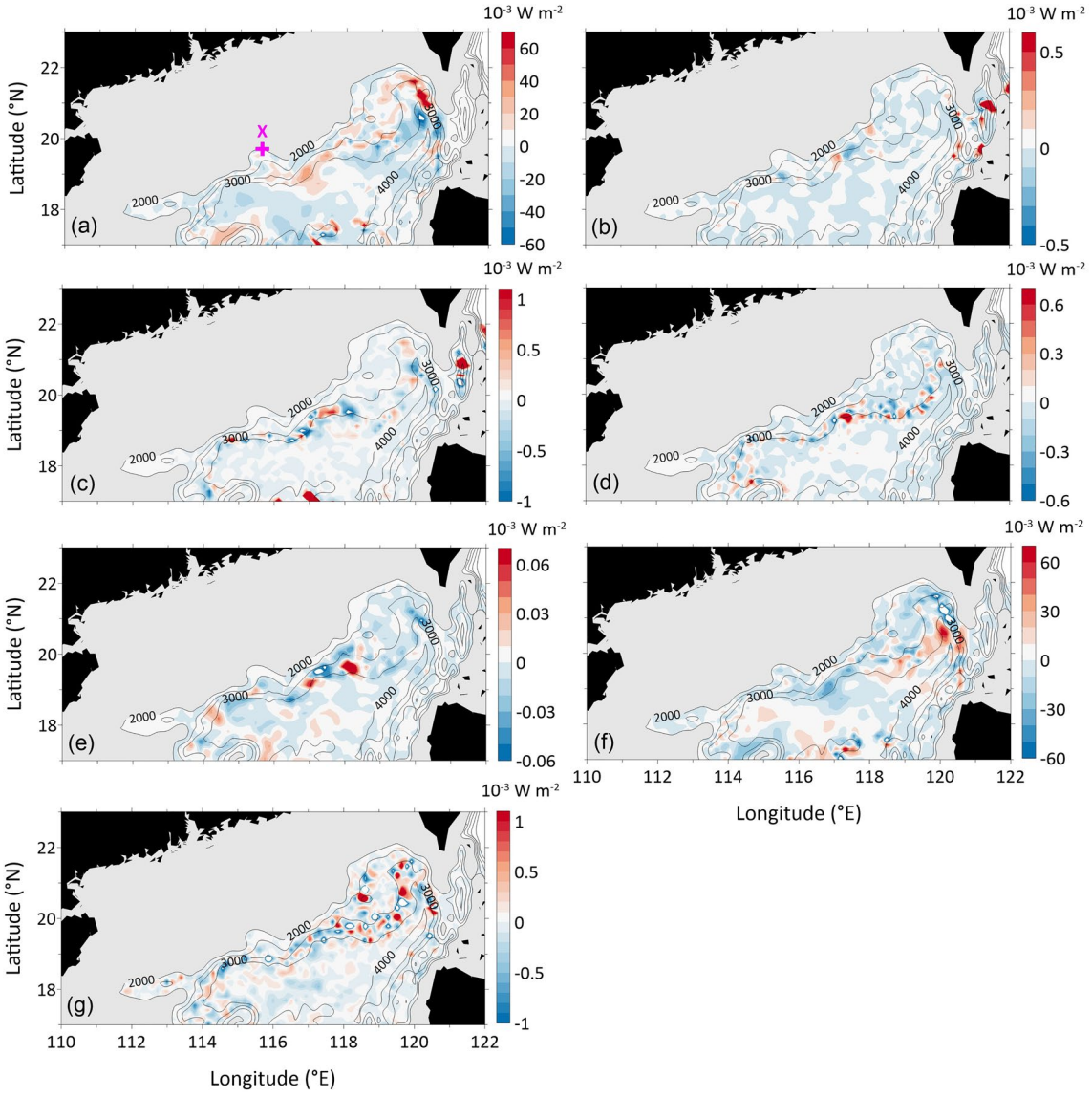

Figure 5. Time-averaged $K^1 + A^1$ energetics (10^{-3} W m^{-2}) integrated from the bottom to 2,000 m for (a) ΔQ_P^1, (b) ΔQ_K^1, (c) ΔQ_A^1, (d) $\Gamma_A^{0\to1}$, (e) $\Gamma_K^{0\to1}$, (f) F_K^1, and (g) F_A^1. Note that the negligibly small transfers between the intraseasonal fluctuation window and the high-frequency oscillation window (i.e., $\Gamma_K^{1\to2}$ and $\Gamma_A^{1\to2}$) are not shown. Areas shallower than 2,000 m are masked. The magenta cross denotes site X.

STD ellipses with major principal axes parallel to the local isobaths are suggestive of TRWs, which have been suggested to contribute greatly to the variability of KE below 2,000 m in the SCS (Quan et al., 2021).

Based on this, we now demonstrate the role of TRWs in deep flow intraseasonal variability. In accordance with Quan et al. (2021), we set three criteria to identify the typical TRWs in the NSCS: (a) the in situ deep KE falling into the TRWs period range (5–90 days) is significant at the 95% confidence level; (b) the spatiotemporal structures of the deep-current fluctuations match the characteristics of TRWs (e.g., vertical coherence and bottom-intensified amplitude); and (c) the frequency and wavenumber conform to the dispersion relation of TRWs (i.e., $\omega = N / \left|\mathbf{K}\right| \cdot \mathbf{K} \times \nabla h$ to leading order). TRWs are identified widely over the continental slopes of the NSCS in the model (Figure 4c) and would require more observations for validation in future studies.

At the TRWs-active locations, the ratios between the STD of the intraseasonal deep KE and the STD of the total deep KE exceed 40% in most regions, and the maximum values can reach 70% over the slopes to the west of the Luzon Strait, southwest of the Dongsha Islands, and northeast of the Xisha Islands. Conversely,

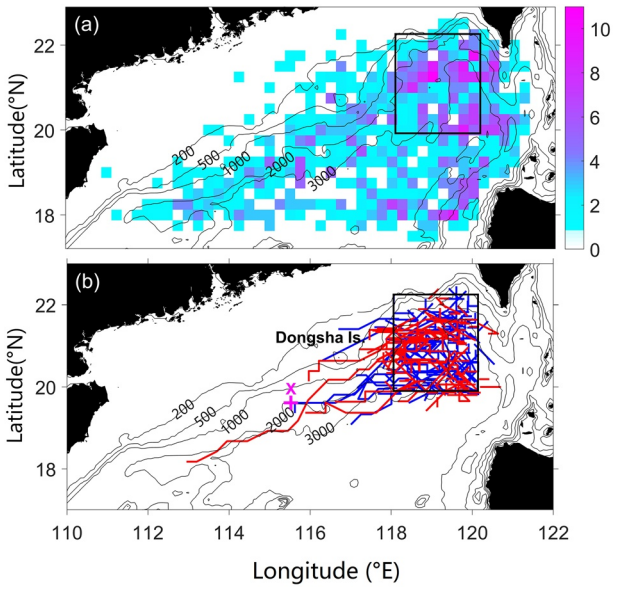

Figure 6. (a) Numbers of mesoscale eddies generated in each 0.25° × 0.25° box during 1993–2019 from the satellite altimeter data. Note that only eddies with a lifespan longer than 30 days are counted. (b) Pathways of anticyclonic (red) and cyclonic (blue) eddies that generated in the Kuroshio intrusion region (black rectangle). The magenta cross denotes site X.

in the regions where TRWs are not identified, intraseasonal variability is not evident, and the ratio is generally lower than 20% (not shown). These results suggest that intraseasonal variability of the deep flow in the NSCS is closely associated with TRWs.

3.2. Energy Source of TRWs-Induced Variability

To identify the energy source of the TRWs-induced oscillations, we examine the intraseasonal energetics of the abyssal NSCS. Using the MS-EVA method described in Section 2.2, the results show that the pressure work dominates the long-term energy budget by at least one order of magnitude larger than other processes (Figure 5). Because the pressure work is closely related to the work done by interfacial form stress, the positive value integrated in the entire domain suggests that the energy source is primarily due to the upper-layer perturbations that can intensively deform the isopycnals. Although the energy from the cross-scale transfers (mainly due to baroclinic instability of the background flow) and advective transports in the deep layer is also considerable during some specific events (Quan et al., 2021), it can be ignored for the long-term integration. Recently, based on the observations in the global ocean and theoretical analysis, de La Lama et al. (2016) and LaCasce (2017) suggested that the quasigeostrophic flow over a sloping topography is significantly surface-intensified and shielded from bottom friction, such that energy must be passed to topographic waves to be dissipated. LaCasce et al. (2019) further demonstrated that the sloping topography can effectively suppress baroclinic instability and the deep flow is predominantly forced by interfacial motions associated with the surface eddies. The relevant mechanism, which is discussed in detail by Quan et al. (2021), can be interpretated as PV conservation or being energized through pressure work in terms of energetics. This is consistent with our findings, as well as a number of other observational and modeling studies in the SCS (Shu et al., 2016; Wang et al., 2019; H. Yang et al., 2013) and Gulf of Mexico (Maslo et al., 2020; Y. Yang et al., 2020), in which energy transfers due to instabilities are largely confined to the upper 1,000 m and pressure work dominates the energetics at depth. In addition, pressure work in the abyssal NSCS is primarily balanced by F_K^1, which is negative integrated in the entire domain and serves as a sink to dissipate energy. This is consistent with the energy pathway from the upper-layer ocean to topography waves through pressure work and then to dissipation. These results highlight the universal dynamics that the net dissipation of energy in the deep ocean is largely supplied through pressure work across layers (Wunsch & Ferrari, 2004), but the detailed pathway connecting the upper and deep layers of the NSCS requires further investigation.

The geographical inhomogeneity of pressure work highlights the spatial differences in the intensity and direction of the energy exchange between layers. The positive pressure work, which acts as a source in the energetics, is mainly located over the continental slopes between Luzon Strait and Dongsha Islands (Figures 5a and 7a), where the Kuroshio intrusion and related eddies are energetic in the upper layer. On the one hand, the periodical meandering of the Kuroshio intrusion can directly radiate energy into the deep layer to excite TRWs, particularly in regions to the northwest of the Luzon Strait (see the elevated positive pressure work along the flow path), wherein the Kuroshio is found to be most unstable on a timescale of 15 days (Zhang et al., 2017). On the other hand, Kuroshio-related eddies can also energize TRWs in the deep layer.

The instability of Kuroshio is thought to dominate the generation of mesoscale eddies to the west of the Luzon Strait (Metzger & Hurlburt, 2001; Nan, Xue, Xiu, et al., 2011; Zhang et al., 2013). Focusing on the region (118°–120°E and 20°–22°N; black rectangle in Figure 6) where the Kuroshio intrusion occurs (Nan, Xue, Chai, et al., 2011), we use satellite altimeter data to detect the eddies generated in this area and their pathways in the NSCS. The results indicate that eddies originating from this region can contribute ~30%

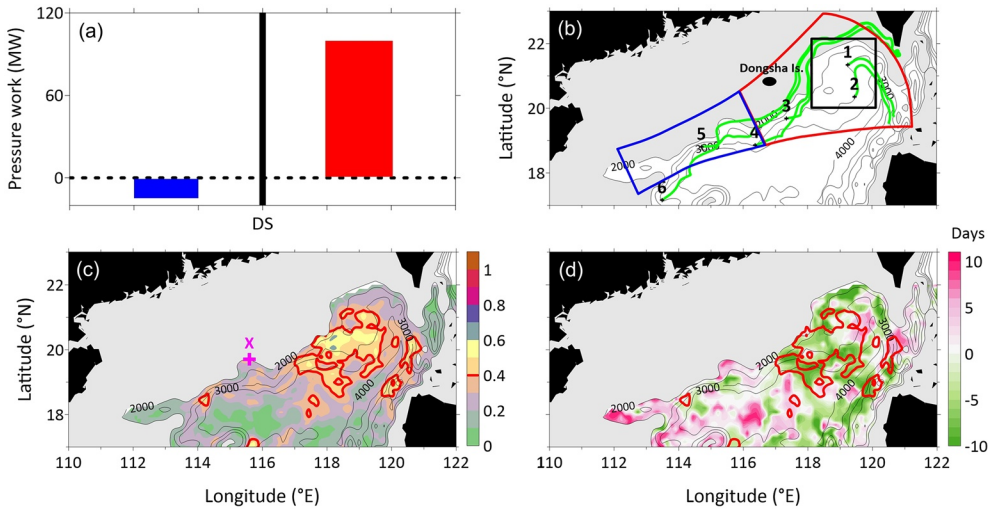

Figure 7. (a) ΔQ_P^1 (MW; 1 MW = 10^6 W) integrated separately in the blue and red parts of the sector in Figure 7a. DS denotes the Dongsha Islands. (b) Topographic Rossby waves rays (green lines) traced from the six sites in Figure 4b backward for 60 days. The sector denotes the areas where the eddies from the Kuroshio intrusion region (black rectangle) can affect. Note that most of these eddies decay to the east of the Dongsha Islands (red part) and only a few can travel to the west (blue part). (c) Maximum lagged correlations of K^1 between the upper and deep layers. Red line marks the 0.4 contour to highlight the areas where the correlation is significant at the 95% confidence level, which is also shown in Figure 7d. (d) Associated time lags (days) corresponding to the maximum correlations. Negative (positive) lag means upper-layer fluctuation leading (lagging) the deep flow. Regions shallower than 2,000 m are masked.

of the total number of eddies in the NSCS during 1993–2019 (Figure 6a). Note that only eddies with a lifespan longer than 30 days are counted. These eddies decay substantially westward. Most of them tend to be trapped by the continental slopes, and only a few can pass the Dongsha Islands (Figure 6b). This Kuroshio-eddy-active region is collocated with the region of elevated positive pressure work shown in Figure 5a, consistent with the downward energy radiation from the upper layer to the deep flow over a sloping topography. Hence, these results suggest that the TRWs on the eastern side of the Dongsha Islands are locally generated by the Kuroshio intrusion and related eddies via pressure work.

In contrast to the eastern side of the Dongsha Islands, the pressure work tends to be negative on the western side (blue bar in Figure 7a), which becomes an energy sink and is unfavorable for the generation of TRWs. This suggests that the TRWs in this region are formed remotely. To determine the origin of these TRWs, we perform a ray tracing analysis against the background of a cyclonic deep circulation (Lan et al., 2013; Wang et al., 2011), as described in Section 2.3. With a time step of 1 h, the backward integrations of the ray tracing model for 60 days at the six sites in Figure 4b show that the TRWs identified over the entire NSCS can, in general, be traced back to the east of the Dongsha Islands (green rays in Figure 7b), which is consistent with the bottom flow shown in Figure 4b and the forward tracing by Quan et al. (2021). Therefore, the TRWs found to the west of the Dongsha Islands are primarily formed on the eastern side.

We further conduct a lead-lag correlation analysis of the intraseasonal KE (i.e., K^1) between the upper and deep layers to highlight the dynamic differences between different regions. In the region to the east of the Dongsha Islands, the deep-layer K^1 shows more significant correlations (higher than 0.4, at the 95% confidence level) with the upper-layer processes that lead by several days, whereas this correlation is not clear in the west (Figures 7c and 7d), which is consistent with the pressure work pattern in Figure 5a and a recent observational study on the coupling of the surface and near-bottom currents in the Gulf of Mexico (Zhu & Liang, 2020).

Taken together, these results suggest that the Kuroshio intrusion and related eddies serve as an important energy source for the TRWs that propagate along the continental slopes through the NSCS and induce substantial intraseasonal variability in the deep flow.

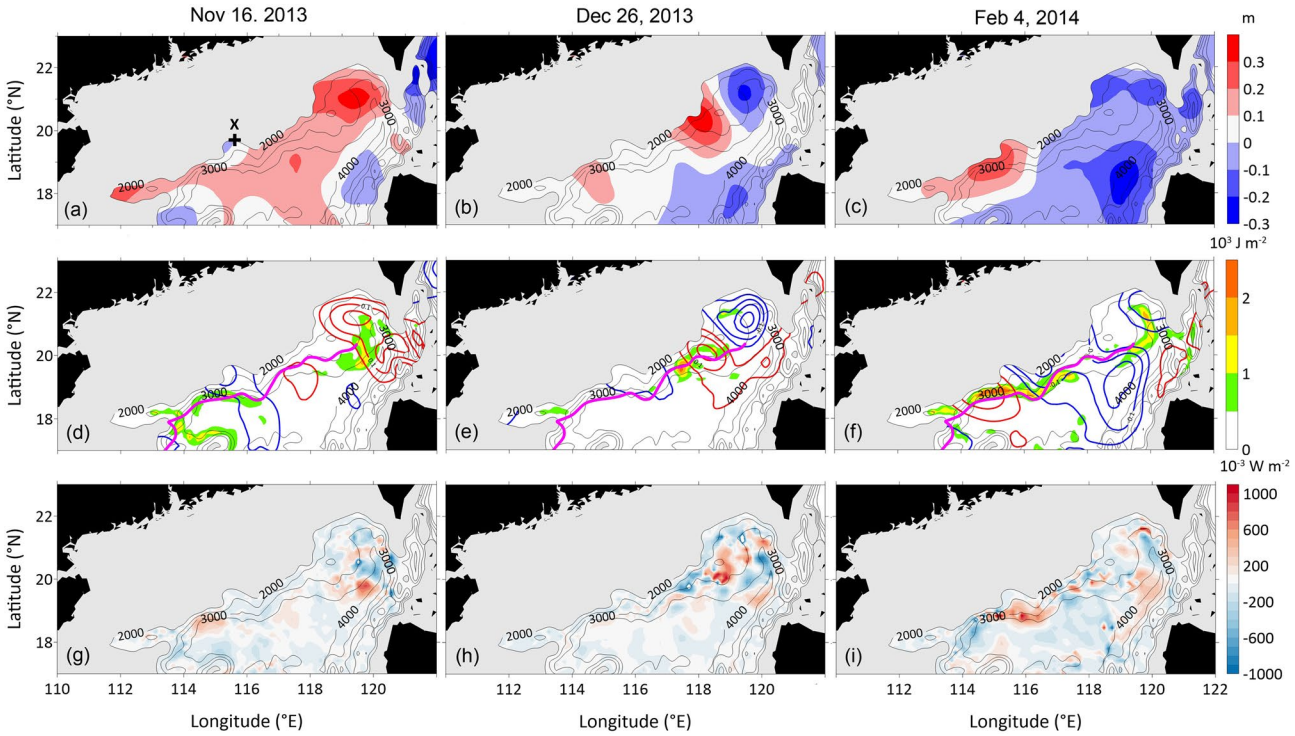

Figure 8. (a–c) Observed sea level anomaly (SLA) (m) from November 16, 2013 to February 04, 2014 with a 40 days interval, derived from satellite altimetry data. Black contours denote isobaths with intervals of 500 m. (d–f) Modeled SLA (colored contours with an interval of 0.05 m) and depth-integrated K^1 (shading; 10^3 J m^{-2}) below 2,000 m during the same period using Hybrid Coordinate Ocean Model GLBv0.08. The magenta line denotes the topographic Rossby waves ray at the period of 48.4 days emanating from the Kuroshio Loop region. (g–i) Corresponding pressure work ΔQ_P^1 (10^{-3} W m^{-2}) integrated from the bottom to 2,000 m. Regions shallower than 2,000 m are masked. Black cross in (a) denotes site X.

3.3. Case Study

To highlight the underlying dynamics, a representative event is considered as an example. Satellite altimeter observed an anticyclonic eddy (AE) shedding from the Kuroshio Loop that began on approximately November 16, 2013 and lasted until February 04, 2014. This AE was the strongest and most long-living Kuroshio-related eddy during the study period (Figures 8a–8c), which was well reproduced in the HYCOM reanalysis (Figures 8d–8f). Unlike most of the Kuroshio-related eddies that disappeared near the Dongsha Islands, this strong AE crossed the NSCS and energized TRWs in the deep layer (the 48.4 days TRW ray is shown for example), with an elevated energy radiation across layers through pressure work along its pathway (Figures 8g–8i).

To further clarify the linkage between the enhanced deep KE to the west of the Dongsha Islands and the surface AE, we calculate a lead-lag correlation between the deep-layer K^1 anomaly at site Y (115°E, 18.9°N; magenta cross in Figure 9a) and those at other locations in the NSCS. The results indicate a significant correlation roughly along the TRW ray emanating from the Kuroshio intrusion region, with the anomaly at site Y lagging the region to the west of the Luzon Strait by approximately 20 days (Figures 9a and 9b). Recently, LaCasce and Groeskamp (2020) suggested that the westward propagation of surface eddies is significantly modulated by sloping topography. Following this study, we solve the linear quasigeostrophic PV equation using a slope bottom condition (LaCasce, 2017) in combination with the typical environmental parameters of the NSCS and obtain the surface mode phase speed for a long planetary Rossby wave as,

$$c = -\beta L_d^2, \tag{6}$$

where $\beta = \partial f / \partial y$ is the planetary beta and L_d is the internal deformation radius. The theoretical phase speed is ~0.1 m s^{-1}, which is close to the propagation speed of the surface AE shown in Figure 9c and the satellite observations by Xu and Oey (2015). According to Rhines (1970), the group speed of TRWs is written as

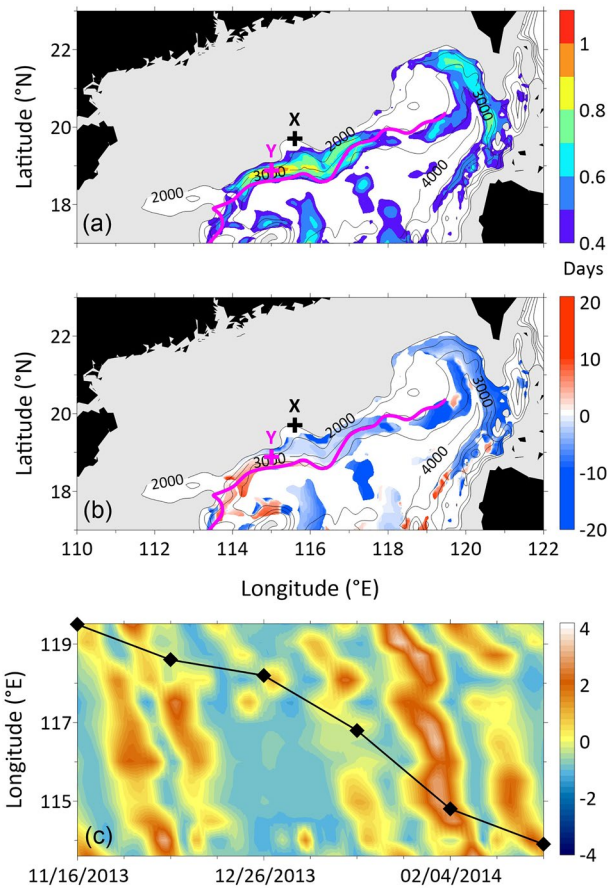

Figure 9. (a) Maximum lagged correlations of deep-layer K^1 anomaly between site Y (magenta cross at 115°E, 18.9°N) and other locations in the northern South China Sea. Only the values over the 95% confidence level and higher than 0.4 are shown. Magenta line indicates the topographic Rossby waves (TRW) ray shown in Figure 8. (b) Associated time lags (days) corresponding to the maximum correlations. Positive (negative) lag means deep-layer K^1 anomaly at site Y leading (lagging) that at other locations. Regions shallower than 2,000 m are masked. (c) Hovmöller plot of the deep-layer K^1 anomaly along the TRW ray shown in (a and b). Note that the results are normalized by extracting the mean value and divided by standard deviation. Diamonds denote the longitudinal locations of the surface anticyclonic eddy in Figure 8.

$$\left|\mathbf{c}_g\right| = \beta_{\text{top}} L_d \left|\cos(\theta)\right| / K, \tag{7}$$

where $\beta_{\text{top}} = f\left|\nabla h\right| / h$ is the topographic beta and θ is the angle between the wavenumber vector and topographic gradient. In the NSCS, $\left|\cos(\theta)\right| / K \geq L_d$ for a long wave and β_{top} overwhelms β on the continental slopes (Quan et al., 2021). Therefore, the normalized deep-layer K^1 anomaly propagated westward along the TRW raypath at a quicker speed of 0.32 m s^{-1} and it took about 20 days to cross the NSCS (Figure 9c), which is consistent with the time lag in the correlation. Because of the faster propagation speed of the TRWs, the deep-layer K^1 was significantly enhanced ahead of the AE along the wave raypath, with the maximum occurring nearly below the eddy (Figures 8d–8f). This event reveals the clear vertical coupling of Kuroshio-related eddy and TRWs-oscillated deep flow.

4. Summary and Discussion

The energy pathway from the open ocean into marginal seas is critical to the redistribution and dissipation of global energy, especially as the latter bridges interocean heat and mass exchange. In this study, observations and high-resolution simulations reveal substantial intraseasonal variability in the deep flow over the continental slopes of the NSCS, which is closely associated with TRWs. Energy budget and ray tracing suggest that the Kuroshio intrusion and related eddies act as an important energy source for TRWs via pressure work. These subinertial waves propagate across the NSCS, causing substantial intraseasonal variability in the deep flow over continental slopes.

This study suggests an energy pathway in the SCS that links the WBC of the upper open ocean to the abyssal marginal sea via TRWs, which could provide an insight to the similar processes in the world oceans, such as the coupling between the Loop Current and deep circulation in the Gulf of Mexico (Tenreiro et al., 2018), as well as the linkage between the surface eddies and the intensified deep ocean variability at the Pacific Yap-Mariana Junction (Ma et al., 2019) and in the Arctic Ocean's Beaufort Gyre (Zhao & Timmermans, 2018). Additionally, our results highlight the role of the Kuroshio intrusion in regulating the SCS circulation throughout the water column. For example, interactions between the TRWs and planetary Rossby waves probably account for the deep upwelling associated with meridional overturning circulation in the abyssal SCS (Shu et al., 2014). Moreover, TRWs and wave-related mixing play a vital role in the generation and evolution of deep circulation in the SCS (Quan & Xue, 2019), as well as in the vertical coupling of the SCS circulation between the upper and middle layers (Quan & Xue, 2018). All these factors may lead to more active SCS circulation that could modulate the Indo-Pacific exchange, thereby affecting the regional climate and ecosystem.

Note that other processes, for example, wind-induced mesoscale perturbations, can also energize TRWs in the deep layer. While this study emphasizes the dynamics that enable remote forcing from the upper open ocean to influence the deep flow in the NSCS, the relative importance of local and remote processes requires further study.

Data Availability Statement

The mooring data are available at https://doi.org/10.6084/m9.figshare.13525838. The HYCOM data can be accessed from https://www.hycom.org/dataserver/gofs-3pt1/analysis. The satellite altimeter data were downloaded from https://resources.marine.copernicus.eu/?option=com_csw&task=results.

Acknowledgments
This study is supported by the National Natural Science Foundation of China (42006007; 41906016; 42006009; 41806023; 41975064), the China Postdoctoral Science Foundation (2020M682767; 2020M681269), the Science and Technology Development Fund, Macau SAR (SKL-IOTSC-2021-2023), the Natural Science Foundation of Guangdong Province (2019A1515011487), and the Fundamental Research Funds for the Central Universities (20184200031610059). The authors appreciate three anonymous reviewers for their insightful comments and Dr. Yukun Qian for discussions that improve this manuscript.

References

Chen, G., Hou, Y., & Chu, X. (2011). Mesoscale eddies in the South China Sea: Mean properties, spatiotemporal variability, and impact on thermohaline structure. *Journal of Geophysical Research*, *116*, C06018. https://doi.org/10.1029/2010jc006716

Cummings, J. A., & Smedstad, O. M. (2013). Variational data assimilation for the global ocean. In *Data assimilation for atmospheric oceanic and hydrologic applications, chapter 13* (Vol. II, pp. 303–343). Springer. https://doi.org/10.1007/978-3-642-35088-7_13

de La Lama, M. S., LaCasce, J. H., & Fuhr, H. K. (2016). The vertical structure of ocean eddies. *Dynamics and Statistics of the Climate System*, *1*, dzw001. https://doi.org/10.1093/climsys/dzw001

Donohue, K. A., Watts, D. R., Hamilton, P., Leben, R., & Kennelly, M. (2016). Loop current eddy formation and baroclinic instability. *Dynamics of Atmosphere and Oceans*, *76*, 195–216. https://doi.org/10.1016/j.dynatmoce.2016.01.004

Ferrari, R., & Wunsch, C. (2009). Ocean circulation kinetic energy: Reservoirs, sources, and sinks. *Annual Review of Fluid Mechanics*, *41*, 253–282. https://doi.org/10.1146/annurev.fluid.40.111406.102139

Gan, J., Liu, Z., & Hui, C. (2016). A three-layer alternating spinning circulation in the South China Sea. *Journal of Physical Oceanography*, *46*, 2309–2315. https://doi.org/10.1175/jpo-d-16-0044.1

Gordon, A. L., Huber, B. A., Metzger, E. J., Susanto, R. D., Hurlburt, H. E., & Adi, T. R. (2012). South China Sea throughflow impact on the Indonesian throughflow. *Geophysical Research Letters*, *39*, L11602. https://doi.org/10.1029/2012gl052021

Hamilton, P. (2009). Topographic Rossby waves in the Gulf of Mexico. *Progress in Oceanography*, *82*, 1–31. https://doi.org/10.1016/j.pocean.2009.04.019

Hamilton, P., Bower, A., Furey, H., Leben, R., & Pérez-Brunius, P. (2019). The loop current: Observations of deep eddies and topographic waves. *Journal of Physical Oceanography*, *49*, 1463–1483. https://doi.org/10.1175/jpo-d-18-0213.1

Johnson, G. C., & Bryden, H. L. (1989). On the size of Antarctic circumpolar current. *Deep-Sea Research*, *36*, 39–53. https://doi.org/10.1016/0198-0149(89)90017-4

LaCasce, J. H. (2017). The prevalence of oceanic surface modes. *Geophysical Research Letters*, *44*, 11097–11105. https://doi.org/10.1002/2017gl075430

LaCasce, J. H., Escartin, J., Chassignet, E. P., & Xu, X. (2019). Jet instability over smooth, corrugated, and realistic bathymetry. *Journal of Physical Oceanography*, *49*, 585–605. https://doi.org/10.1175/jpo-d-18-0129.1

LaCasce, J. H., & Groeskamp, S. (2020). Baroclinic modes over rough bathymetry and the surface deformation radius. *Journal of Physical Oceanography*, *50*, 2835–2847. https://doi.org/10.1175/jpo-d-20-0055.1

Lan, J., Zhang, N., & Wang, Y. (2013). On the dynamics of the South China Sea deep circulation. *Journal of Geophysical Research: Oceans*, *118*, 1206–1210. https://doi.org/10.1002/jgrc.20104

Liang, X. S. (2016). Canonical transfer and multiscale energetics for primitive and quasigeostrophic atmospheres. *Journal of the Atmospheric Sciences*, *73*, 4439–4468. https://doi.org/10.1175/jas-d-16-0131.1

Liang, X. S., & Anderson, D. G. M. (2007). Multiscale window transform. *Multiscale Modeling & Simulation*, *6*, 437–467. https://doi.org/10.1137/06066895x

Liang, X. S., & Robinson, A. R. (2005). Localized multiscale energy and vorticity analysis. I: Fundamentals. *Dynamics of Atmospheres and Oceans*, *38*, 195–230. https://doi.org/10.1016/j.dynatmoce.2004.12.004

Liang, X. S., & Robinson, A. R. (2007). Localized multi-scale energy and vorticity analysis. II: Finite-amplitude instability theory and validation. *Dynamics of Atmospheres and Oceans*, *44*, 51–76. https://doi.org/10.1016/j.dynatmoce.2007.04.001

Liang, X. S., & Robinson, A. R. (2009). Multiscale processes and nonlinear dynamics of the circulation and upwelling events off Monterey Bay. *Journal of Physical Oceanography*, *39*, 290–313. https://doi.org/10.1175/2008jpo3950.1

Luecke, C. A., Arbic, B. K., Bassette, S. L., Richman, J. G., Shriver, J. F., Alford, M. H., et al. (2017). The global mesoscale eddy available potential energy field in models and observations. *Journal of Geophysical Research: Oceans*, *122*, 9126–9143. https://doi.org/10.1002/2017jc013136

Ma, J., & Liang, X. S. (2017). Multiscale dynamical processes underlying the wintertime Atlantic blockings. *Journal of the Atmospheric Sciences*, *74*, 3815–3831. https://doi.org/10.1175/jas-d-16-0295.1

Ma, Q., Wang, F., Wang, J., & Lyu, Y. (2019). Intensified deep ocean variability induced by topographic Rossby waves at the Pacific Yap-Mariana junction. *Journal of Geophysical Research: Oceans*, *124*, 8360–8374. https://doi.org/10.1029/2019jc015490

Magalhães, F. C., Azevedo, J. L. L., & Oliveira, L. R. (2017). Energetics of eddy-mean flow interactions in the Brazil current between 20°S and 36°S. *Journal of Geophysical Research: Oceans*, *122*, 6129–6146. https://doi.org/10.1002/2016jc012609

Maslo, A., De Souza, J. M. A. C., & Pardo, J. S. (2020). Energetics of the deep Gulf of Mexico. *Journal of Physical Oceanography*, *50*, 1655–1675. https://doi.org/10.1175/jpo-d-19-0308.1

Meinen, C., Fields, E., Pickart, R. S., & Watts, D. R. (1993). Ray tracing on topographic Rossby waves. *Graduate School of Oceanography Technical Report 93-1, University of Rhode Island*, (pp. 1–43).

Metzger, E. J., & Hurlburt, H. E. (2001). The nondeterministic nature of Kuroshio penetration and eddy shedding in the South China Sea. *Journal of Physical Oceanography*, *31*, 1712–1732. https://doi.org/10.1175/1520-0485(2001)031<1712:tnnokp>2.0.co;2

Nan, F., Xue, H., Chai, F., Shi, L., Shi, M., & Guo, P. (2011). Identification of different types of Kuroshio intrusion into the South China Sea. *Ocean Dynamics*, *61*, 1291–1304. https://doi.org/10.1007/s10236-011-0426-3

Nan, F., Xue, H., Xiu, P., Chai, F., Shi, M., & Guo, P. (2011). Oceanic eddy formation and propagation southwest of Taiwan. *Journal of Geophysical Research*, *116*, C12045. https://doi.org/10.1029/2011jc007386

Nan, F., Xue, H., & Yu, F. (2015). Kuroshio intrusion into the South China Sea: A review. *Progress in Oceanography*, *137*, 314–333. https://doi.org/10.1016/j.pocean.2014.05.012

Oey, L. Y. (2008). Loop current and deep eddies. *Journal of Physical Oceanography*, *38*, 1426–1449. https://doi.org/10.1175/2007jpo3818.1

Oey, L. Y., & Lee, H. C. (2002). Deep eddy energy and topographic Rossby waves in the Gulf of Mexico. *Journal of Physical Oceanography*, *32*, 3499–3527. https://doi.org/10.1175/1520-0485(2002)032<3499:deeatr>2.0.co;2

Pickart, R. S. (1995). Gulf Stream-generated topographic Rossby waves. *Journal of Physical Oceanography*, *25*, 574–586. https://doi.org/10.1175/1520-0485(1995)025<0574:gstrw>2.0.co;2

Qu, T., Du, Y., & Sasaki, H. (2006). South China Sea throughflow: A heat and freshwater conveyor. *Geophysical Research Letters*, *33*, L23617. https://doi.org/10.1029/2006gl028350

Qu, T., Song, Y. T., & Yamagata, T. (2009). An introduction to the South China Sea throughflow: Its dynamics, variability, and application for climate. *Dynamics of Atmospheres and Oceans*, *47*, 3–14. https://doi.org/10.1016/j.dynatmoce.2008.05.001

Quan, Q., Cai, Z., Jin, G., & Liu, Z. (2021). Topographic Rossby waves in the abyssal South China Sea. *Journal of Physical Oceanography*, *51*, 1795–1812.

Quan, Q., & Xue, H. (2018). Layered model and insights into the vertical coupling of the South China Sea circulation in the upper and middle layers. *Ocean Modelling*, *129*, 75–92. https://doi.org/10.1016/j.ocemod.2018.06.006

Quan, Q., & Xue, H. (2019). Influence of abyssal mixing on the multilayer circulation in the South China Sea. *Journal of Physical Oceanography*, *49*, 3045–3060. https://doi.org/10.1175/jpo-d-19-0020.1

Quan, Q., Xue, H., Qin, H., Zeng, X., & Peng, S. (2016). Features and variability of the South China Sea western boundary current from 1992 to 2011. *Ocean Dynamics*, *66*, 795–810. https://doi.org/10.1007/s10236-016-0951-1

Rhines, P. B. (1970). Edge-, bottom-, and Rossby waves in a rotating stratified fluid. *Geophysical and Astrophysical Fluid Dynamics*, *1*, 273–302. https://doi.org/10.1080/03091927009365776

Shu, Y., Wang, Q., & Zu, T. (2018). Progress on shelf and slope circulation in the northern South China Sea. *Science China Earth Sciences*, *61*, 560–571. https://doi.org/10.1007/s11430-017-9152-y

Shu, Y., Xue, H., Wang, D., Chai, F., Xie, Q., Cai, S., et al. (2016). Persistent and energetic bottom-trapped topographic Rossby waves observed in the southern South China Sea. *Scientific Reports*, *6*, 24338. https://doi.org/10.1038/srep24338

Shu, Y., Xue, H., Wang, D., Chai, F., Xie, Q., Yao, J., & Xiao, J. (2014). Meridional overturning circulation in the South China Sea envisioned from the high-resolution global reanalysis data GLBa0.08. *Journal of Geophysical Research: Oceans*, *119*, 3012–3028. https://doi.org/10.1002/2013jc009583

Sun, Z., Zhang, Z., Qiu, B., Zhang, X., Zhou, C., Huang, X., et al. (2020). Three-dimensional structure and interannual variability of the Kuroshio loop current in the northeastern South China Sea. *Journal of Physical Oceanography*, *50*, 2437–2455. https://doi.org/10.1175/jpo-d-20-0058.1

Tenreiro, M., Candela, J., Sanz, E. P., Sheinbaum, J., & Ochoa, J. (2018). Near-surface and deep circulation coupling in the western Gulf of Mexico. *Journal of Physical Oceanography*, *48*, 145–161. https://doi.org/10.1175/jpo-d-17-0018.1

Tian, F., Wu, D., Yuan, L., & Chen, G. (2020). Impacts of the efficiencies of identification and tracking algorithms on the statistical properties of global mesoscale eddies using merged altimeter data. *International Journal of Remote Sensing*, *41*, 2835–2860. https://doi.org/10.1080/01431161.2019.1694724

Tian, J., Yang, Q., Liang, X., Xie, L., Hu, D., Wang, F., & Qu, T. (2006). Observation of Luzon Strait transport. *Geophysical Research Letters*, *33*, L19607. https://doi.org/10.1029/2006gl026272

Wang, G., Xie, S., Qu, T., & Huang, R. (2011). Deep South China Sea circulation. *Geophysical Research Letters*, *38*, L05601. https://doi.org/10.1029/2010gl046626

Wang, Q., Zeng, L., Chen, J., He, Y., Zhou, W., & Wang, D. (2020). The linkage of Kuroshio intrusion and mesoscale eddy variability in the northern South China Sea: Subsurface speed maximum. *Geophysical Research Letters*, *46*, e2020GL087034. https://doi.org/10.1029/2020GL087034

Wang, Q., Zeng, L., Shu, Y., Li, J., Chen, J., He, Y., et al. (2019). Energetic topographic Rossby waves in the northern South China Sea. *Journal of Physical Oceanography*, *49*, 2697–2714. https://doi.org/10.1175/jpo-d-18-0247.1

Wang, Q., Zeng, L., Shu, Y., Liu, Q., Zu, T., Li, J., et al. (2020). Interannual variability of South China Sea winter circulation: Response to Luzon Strait transport and El Niño wind. *Climate Dynamics*, *54*, 1145–1159. https://doi.org/10.1007/s00382-019-05050-2

Wang, Q., Zhou, W., Zeng, L., Chen, J., He, Y., & Wang, D. (2020). Intraseasonal variability of cross-slope flow in the northern South China Sea. *Journal of Physical Oceanography*, *50*, 2071–2084. https://doi.org/10.1175/jpo-d-19-0293.1

Wei, J., Li, M. T., Malanotte-Rizzoli, P., Gordon, A. L., & Wang, D. (2016). Opposite variability of Indonesian throughflow and South China Sea throughflow in the Sulawesi Sea. *Journal of Physical Oceanography*, *46*, 3165–3180. https://doi.org/10.1175/jpo-d-16-0132.1

Wunsch, C., & Ferrari, R. (2004). Vertical mixing, energy, and the general circulation of the oceans. *Annual Review of Fluid Mechanics*, *36*, 281–314. https://doi.org/10.1146/annurev.fluid.36.050802.122121

Xiu, P., Chai, F., Shi, L., Xue, H., & Chao, Y. (2010). A census of eddy activities in the South China Sea during 1993–2007. *Journal of Geophysical Research*, *115*, C03012. https://doi.org/10.1029/2009jc005657

Xu, F., & Oey, L. Y. (2015). Seasonal SSH variability of the northern South China Sea. *Journal of Physical Oceanography*, *45*, 1595–1609. https://doi.org/10.1175/jpo-d-14-0193.1

Xue, H., Chai, F., Pettigrew, N., Xu, D., Shi, M., & Xu, J. (2004). Kuroshio intrusion and the circulation in the South China Sea. *Journal of Geophysical Research*, *109*, C02017. https://doi.org/10.1029/2002jc001724

Yang, H., Wu, L., Liu, H., & Yu, Y. (2013). Eddy energy sources and sinks in the South China Sea. *Journal of Geophysical Research: Oceans*, *118*, 4716–4726. https://doi.org/10.1002/jgrc.20343

Yang, Q., Tian, J., & Zhao, W. (2010). Observation of Luzon Strait transport in summer 2007. *Deep-Sea Research I*, *57*, 670–676. https://doi.org/10.1016/j.dsr.2010.02.004

Yang, Y., & Liang, X. S. (2016). The instabilities and multiscale energetics underlying the mean-interannual-eddy interactions in the Kuroshio extension region. *Journal of Physical Oceanography*, *46*, 1477–1494. https://doi.org/10.1175/jpo-d-15-0226.1

Yang, Y., & Liang, X. S. (2018). On the seasonal eddy variability in the Kuroshio extension. *Journal of Physical Oceanography*, *48*, 1675–1689. https://doi.org/10.1175/jpo-d-18-0058.1

Yang, Y., Weisberg, R. H., Liu, Y., & Liang, X. S. (2020). Instabilities and multiscale interactions underlying the loop current eddy shedding in the Gulf of Mexico. *Journal of Physical Oceanography*, *50*, 1289–1317. https://doi.org/10.1175/jpo-d-19-0202.1

Yu, Z., Shen, S., McCreary, J. P., Yaremchuk, M., & Furue, R. (2007). South China Sea throughflow as evidenced by satellite images and numerical experiments. *Geophysical Research Letters*, *34*, L01601. https://doi.org/10.1029/2006gl028103

Zhang, Z., Zhao, W., Qiu, B., & Tian, J. (2017). Anticyclonic eddy sheddings from Kuroshio Loop and the accompanying cyclonic eddy in the northeastern South China Sea. *Journal of Physical Oceanography*, *47*, 1243–1259. https://doi.org/10.1175/jpo-d-16-0185.1

Zhang, Z., Zhao, W., Tian, J., & Liang, X. (2013). A mesoscale eddy pair southwest of Taiwan and its influence on deep circulation. *Journal of Geophysical Research: Oceans*, *118*, 6479–6494. https://doi.org/10.1002/2013jc008994

Zhang, Z., Zhao, W., Tian, J., Yang, Q., & Qu, T. (2015). Spatial structure and temporal variability of the zonal flow in the Luzon Strait. *Journal of Geophysical Research: Oceans*, *120*, 759–776. https://doi.org/10.1002/2014jc010308

Zhao, B., & Timmermans, M.-L. (2018). Topographic Rossby waves in the Arctic Ocean's Beaufort Gyre. *Journal of Geophysical Research: Oceans*, *123*, 6521–6530. https://doi.org/10.1029/2018jc014233

Zhu, Y., & Liang, X. F. (2020). Coupling of the surface and near-bottom currents in the Gulf of Mexico. *Journal of Geophysical Research: Oceans*, *125*, e2020JC016488. https://doi.org/10.1029/2020jc016488